Analysis of Formation Flying in Eccentric Orbits Using Linearized Equations of Relative Motion

Christopher Lane* and Penina Axelrad†
Colorado Center for Astrodynamics Research, University of Colorado, Boulder, CO 80309

Geometrical methods for formation flying design based on the analytical solution to Hill's equations have been previously developed and used to specify desired relative motions in near circular orbits. By generating relationships between the vehicles that are intuitive, these approaches offer valuable insight into the relative motion and allow for the rapid design of satellite configurations to achieve mission specific requirements, such as vehicle separation at perigee or apogee, minimum separation, or a specific geometrical shape. Furthermore, the results obtained using geometrical approaches can be used to better constrain numerical optimization methods; allowing those methods to converge to optimal satellite configurations faster. This paper presents a set of geometrical relationships for formations in eccentric orbits, where Hill's equations are not valid, and shows how these relationships can be used to investigate formation designs and how they evolve with time.

I. Introduction

A great deal of attention in recent years has been focused on various ways to improve our ability to describe the motion of one vehicle about another (see Alfriend and Yan[1]). Broucke[2], Alfriend and Gim[3], Lawden[6], Melton[8], and Tschauner and Hempel[11] all derived equations of relative motion valid for vehicles in nearby eccentric orbits and Alfriend and Gim[3] and Schweighart and Sedwick[10] included first-order perturbation effects in their relative motion equations. This paper focuses on formation design in unperturbed, eccentric orbits using geometrical relationships derived from the relative motion equations described in Ref. 2, which are completely explicit in time. Note the relative motion equations developed in Refs. 3, 6, 8, and 11 all use true anomaly as the independent variable or are in the form of a series expansion in eccentricity.

Previous geometrical methods for formation design and station-keeping, such as those proposed by Lovell and Tragesser[7] and Sabol et al[9], are based on the analytical solution to Hill's equations[4], which limits their applicability to near-circular reference orbits. Recently, Hughes[5] published a numerical optimization method for formation design in eccentric orbits that maximizes a mission performance metric. While numerical optimization methods are necessary to maximize the performance of any mission, if used exclusively, they have several limitations. First, numerical optimization methods require a realistic initial guess (or guesses) of the optimal satellite configuration to avoid numerical instability problems. Developing a realistic initial guess requires some knowledge of the relative motion and the feasibility of a desired satellite configuration. Second, it is difficult to characterize how the properties of the relative motion are related to desired formation parameters. This relationship is typically explored in a brute-force manner: the relative motion properties for many different values of a design parameter are examined until the relationship between the two is understood.

Alternatively, geometrical methods can be used to quickly design satellite configurations that achieve specific mission requirements. They offer an intuitive understanding of the relationship between the properties of the relative motion and desired formation parameters and the ability to visualize the relative motion without a simulation, a valuable tool early in the design process. Thus, the two methods compliment each other if used in conjunction. A geometrical design method that is not limited to near circular reference orbits is, therefore, desired.

* Graduate Student, Aerospace Engineering Sciences, The University of Colorado-Boulder, 431 UCB, Boulder, CO 80309-0431. E-mail: christopher.lane@colorado.edu.
† Associate Professor, Aerospace Engineering Sciences, The University of Colorado-Boulder, 431 UCB, Boulder, CO 80309-0431. E-mail: penina.axelrad@colorado.edu.

Beginning with the recently published analytical solutions to the linearized equations of relative motion in an eccentric reference orbit provided in Ref. 2, we have developed a set of geometrical relationships for formations in eccentric orbits. These relationships allow for the use of intuitive design and station-keeping methods, similar to those discussed in Refs. 7 and 9, to be used to specify formation parameters. As an added benefit, these relationships directly relate initial conditions to Keplerian elements, eliminating some of the coordinate transformations necessary in other geometrical methods.

The remainder of this paper develops the set of geometrical relationships for formations in eccentric orbits, shows how these relationships can be used for formation design, and, finally, examines the validity and accuracy of the proposed design methods for three test formations.

II. Linearized Equations of Relative Motion in Elliptic Reference Orbit

Recently, Ref. 2 presented a time-explicit solution to the linearized equations of motion of nearby objects in eccentric orbits. The linearization assumes only that the two objects are proximate in position and velocity, but does not require any assumptions about the eccentricity of the orbit. The equations are described in terms of the relative position and velocity of a deputy (Ref. 2 refers to this as the chaser) with respect to a chief (called the target in Ref. 2) expressed in a curvilinear Local-Vertical-Local-Horizontal (LVLH) coordinate frame.

This frame moves with the chief and will be referred to as the RAC (radial, along-track, and cross-track) frame in this paper. Figure 1 shows the system. The R axis is aligned with the position vector of the chief and the C axis is normal to the orbital plane of the chief. The A axis is perpendicular to the other two axes and its direction is defined by $C \times R$. The R axis is a linear dimension; motions along the A and C axes are measured on a sphere that is locally tangent to the orbit of the chief at every instant in time (Fig. 1). The radius of the sphere is equal to the instantaneous position of the chief. The rotation rate of the frame is time varying. The use of this frame, instead of a more conventional Cartesian frame, dramatically improves the accuracy of the following analysis.

The relative equations of motion in terms of the radial position (x) and velocity, along-track position (y) and velocity, and cross-track position (z) and velocity, are given as

$$\ddot{x} - 2\dot{\theta}\,\dot{y} - \dot{\theta}^2 x - \ddot{\theta}\,y = 2\left(\mu/r^3\right)x, \tag{1}$$

$$\ddot{y} + 2\dot{\theta}\,\dot{x} - \dot{\theta}^2 y + \ddot{\theta}\,x = -\left(\mu/r^3\right)y, \tag{2}$$

$$\ddot{z} = -\left(\mu/r^3\right)z. \tag{3}$$

The time varying coefficients in Eqs. (1) – (3) are expressed as

$$r = \frac{a\left(1-e^2\right)}{1+e\cos\nu},\ \dot{\theta} = \frac{na^2}{r^2}\sqrt{1-e^2},\ \ddot{\theta} = \frac{-2\mu e\sin\nu}{r^3},$$

where v is the true anomaly of the chief.

In Ref. 2, the solution to Eqs. (1) and (2), the coplanar motion of the deputy, is derived by referencing the relative position and velocity to relative Keplerian elements. Specifically, Ref. 2 considers the semimajor axis a, eccentricity e, argument of perigee ω, and mean anomaly at epoch M_0. Because we are also interested in out-of-plane motion, we consider the inclination i and the right ascension of the ascending node Ω as well. Indicating the parameters of the orbit of the chief with no subscripts, we have

$$a_{deputy} = a + \Delta a,\ e_{deputy} = e + \Delta e,\ \omega_{deputy} = \omega + \Delta\omega,\ M_{deputy0} = M_0 + \Delta M,$$
$$i_{deputy} = i + \Delta i,\ \Omega_{deputy} = \Omega + \Delta\Omega,$$

where Δa, Δe, $\Delta\omega$, ΔM, Δi, and $\Delta\Omega$ represent small deviations from the Keplerian elements of the chief. The exact solution to Eqs. (1) – (3) is expressed in terms of the Keplerian element differences as follows

$$x = \left(\frac{r}{a} - \frac{3n(t-t_0)e\sin\nu}{2\sqrt{1-e^3}} \right) \Delta a - a\cos\nu\Delta e + \frac{ae\sin\nu}{\sqrt{1-e^2}} \Delta M, \tag{4}$$

$$y = \left(-\frac{3a}{2r} n(t-t_0)\sqrt{1-e^2} \right) \Delta a + \left(a + \frac{r}{1-e^2} \right) \sin\nu\Delta e + \frac{a^2}{r}\sqrt{1-e^2}\,\Delta M + r(\Delta\omega + \cos i\Delta\Omega), \tag{5}$$

$$z = r\sin(\omega+\nu)\Delta i - r\sin i\cos(\omega+\nu)\Delta\Omega. \tag{6}$$

Note in Ref. 2 the expression for the along-track position, y, does not include a dependence on $\Delta\Omega$ by *definition* because only coplanar motion of the deputy is considered and, for the out-of-plane motion to be zero, $\Delta\Omega$ (and Δi) must be zero. To understand what causes the along-track dependence on $\Delta\Omega$, consider the case when $\Delta\Omega \neq 0$ so that $\Omega_{deputy} \neq \Omega$, as illustrated in Fig. 2. In this case, the argument of perigee of the chief and deputy are measured in slightly different planes and this causes an offset between the chief and deputy in the along-track direction.

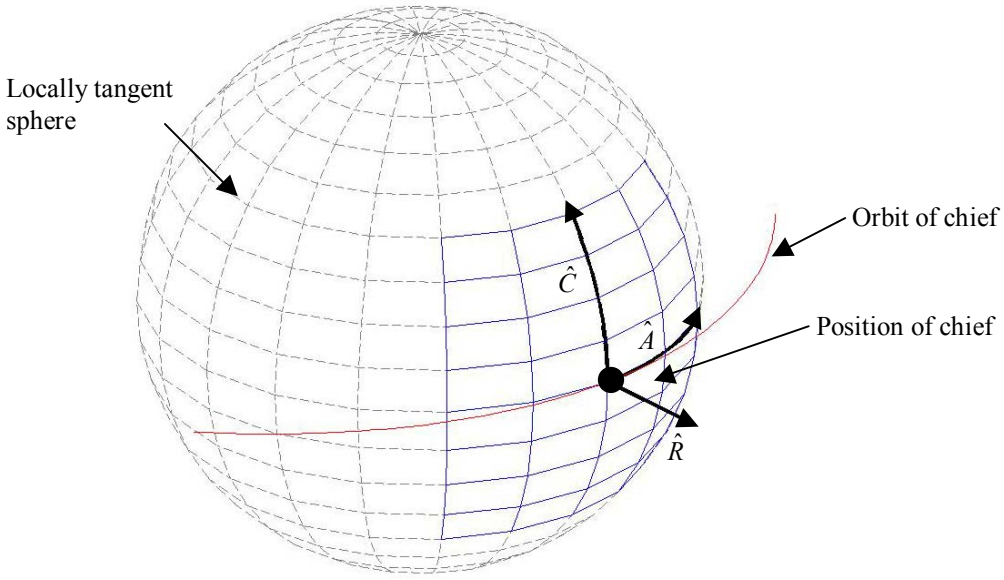

Figure 1. The RAC frame.

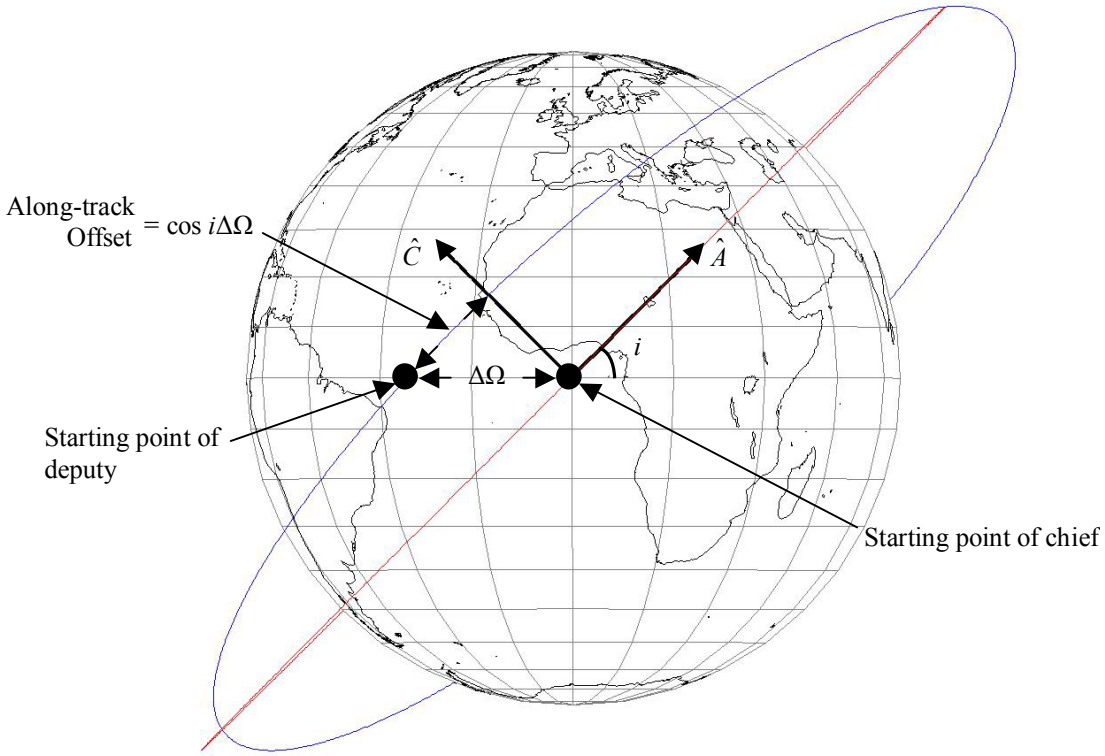

Figure 2. Effect of nodal difference on along-track position.

III. Geometry of Relative Motion in Elliptical Reference Orbit

Beginning with Eqs. (4) – (6), we have established a set of geometrical relationships that describe, in an accessible way, the relative motion in an eccentric orbit. The goal was to create a simple set of descriptors, such as those used by Vallado[12], which describe the motion of a deputy about a chief in an eccentric orbit.

Because we are primarily interested in establishing stable formations, we first eliminate the possibility of secular growth in the separation between vehicles by constraining the energy of both orbits to be equal (i.e, $\Delta a = 0$). We are left with

$$x = -a\cos\nu\Delta e + \frac{ae\sin\nu}{\sqrt{1-e^2}}\Delta M, \tag{7}$$

$$y = \left(a + \frac{r}{1-e^2}\right)\sin\nu\Delta e + \frac{a^2}{r}\sqrt{1-e^2}\,\Delta M + r\left(\Delta\omega + \cos i\Delta\Omega\right), \tag{8}$$

$$z = r\sin(\omega+\nu)\Delta i - r\sin i\cos(\omega+\nu)\Delta\Omega. \tag{9}$$

Note that all the terms in Eqs. (7) – (9) have an implicit dependence on time. With some algebraic manipulation, we can write Eqs. (7) – (9) as

$$x = C\sin(\nu - \psi_0), \tag{10}$$

$$y = C\cos(\nu - \psi_0) - D\cos(E + \gamma_0) + y_{cm}, \tag{11}$$

$$z = G\sin(E + \varphi_0) + z_{cm}, \tag{12}$$

where E is the eccentric anomaly of the chief, y_{cm} is the along-track center of motion, z_{cm} is the cross-track center of motion, and the constants are defined as

$$C = a\sqrt{\Delta e^2 + \frac{e^2 \Delta M^2}{1-e^2}},\ D = a\sqrt{\frac{\Delta e^2}{1-e^2} + e^2\left(\cos i\Delta\Omega + \Delta\omega\right)^2},\ G = a\sqrt{\alpha^2 + \beta^2},$$

$$\alpha = \sin\omega\Delta i - \sin i\cos\omega\Delta\Omega,\ \beta = \sqrt{1-e^2}\left(\cos\omega\Delta i + \sin i\sin\omega\Delta\Omega\right),$$

$$y_{cm} = a\left(\frac{\Delta M}{\sqrt{1-e^2}} + \cos i\Delta\Omega + \Delta\omega\right),\ z_{cm} = -ae\alpha,$$

$$\sin\psi_0 = \frac{a\Delta e}{C},\ \cos\psi_0 = \frac{ae\Delta M}{C\sqrt{1-e^2}},$$

$$\sin\gamma_0 = \frac{a\Delta e}{D\sqrt{1-e^2}},\ \cos\gamma_0 = \frac{ae\left(\cos i\Delta\Omega + \Delta\omega\right)}{D},$$

$$\sin\varphi_0 = \frac{a\alpha}{G},\ \cos\varphi_0 = \frac{a\beta}{G}.$$

The geometrical structure of Eqs. (10) – (12) can be used to investigate formation designs and how they evolve with time.

IV. Formation Design

Inspection of Eqs. (10) – (12) reveals that, in general, the relative motion in an eccentric orbit will *not* be an ellipse in any plane. This is a significant departure (and complication) from the analytical solution to Hill's equations[4], where the motion in the radial/along-track plane is always a 2x1 ellipse with the major axis in the along-track direction. We will show later that elliptical motion is possible in the along-track/cross-track plane, but only when certain constraints are imposed on the motion (elliptical motion is also possible in the radial/along-track plane). The non-elliptical motion is due to the eccentricity of the reference orbit. In an eccentric orbit, $E \neq \nu$, except at perigee and apogee, and, thus, the terms that vary with eccentric anomaly have a different time dependence than those that vary with true anomaly.

Five design parameters must be specified in Eqs. (10) – (12) in addition to the constraint that $\Delta a = 0$ to eliminate the possibility of secular growth between the vehicles. Three of the parameters, Δe, $\Delta\omega$, and ΔM, only affect the coplanar motion (i.e., radial/along-track motion) and Δi only affects the out-of-plane motion (i.e., cross-track motion). Both the coplanar and out-of-plane motion is affected by $\Delta\Omega$.

In the following sections, three types of formations are examined: (1) an along-track formation, (2) a follower formation, and (3) an along-track/cross-track formation. The design of each formation is described in detail below.

A. Along-track Formations

Purely along-track motion is achieved by requiring the radial and cross-track positions always be zero. Thus, C, G, and z_{cm} must be zero in Eqs. (10) – (12). This is achieved by requiring $\Delta e = \Delta M = \Delta i = \Delta\Omega = 0$. The only parameter to specify in an along-track formation design is $\Delta\omega$, which allows us to specify a desired along-track separation at a particular time in the orbit. For example, we can create a desired separation of ρ_0 at perigee by setting

$$\Delta\omega_{AF} = \frac{\rho_0}{a(1-e)}, \tag{13}$$

or at apogee by setting

$$\Delta\omega_{AF} = \frac{\rho_A}{a(1+e)},$$

where ρ_A is the desired separation at apogee.

The minimum separation, $\rho_{\min}^{AF}$, between two vehicles in an along-track formation occurs at perigee ($\nu_{\min}^{AF}$ = 0-deg) and is equal to

$$\rho_{\min}^{AF} = a\Delta\omega_{AF}(1-e). \tag{14}$$

Similarly, the maximum separation, $\rho_{\max}^{AF}$, occurs at apogee ($\nu_{\max}^{AF}$ = 180-deg) and is equal to

$$\rho_{\max}^{AF} = a\Delta\omega_{AF}(1+e). \tag{15}$$

B. Follower Formations

A follower formation is a formation of vehicles that share the same groundtrack. For two vehicles to occupy the same groundtrack, they must pass over the same set of points on the Earth. The important consideration here is that the nodal separation, $\Delta\Omega$, must account for ΔM and the rotation rate of the Earth, W_e. In particular,

$$\Delta\Omega_{FF} = -W_e \frac{\Delta M_{FF}}{n}, \tag{16}$$

where n is the mean motion of the reference orbit (a detailed derivation of this relationship is provided in Ref. 9). It should be noted that Eq. (16) is only applicable when $\Delta a = 0$. If $\Delta a \neq 0$, then n for each vehicle is different and Eq. (16) is no longer valid.

All the vehicles in a follower formation must have the same eccentricity, inclination, and argument of perigee if they are to share the same groundtrack. Thus $\Delta e = \Delta i = \Delta\omega = 0$. The only free parameter in a follower formation design is ΔM, which represents a desired separation at a particular time in the orbit. We can create a separation of ρ_0 at perigee by setting

$$\Delta M_{FF} = \pm\frac{\rho_0}{a}\left[\left(\frac{1+e}{\sqrt{1-e^2}} - \frac{(1-e)\cos iW_e}{n}\right)^2 + \frac{\cos^2\omega\sin^2 iW_e^2(1-e)^2}{n^2}\right]^{-1/2}, \tag{17}$$

where the ± indicates whether the second vehicle is ahead (+) or behind (−) the reference vehicle. Substituting Eq. (17) back into Eq. (16) gives

$$\Delta\Omega_{FF} = \mp\frac{W_e\rho_0}{\sqrt{\mu/a}}\left[\left(\frac{1+e}{\sqrt{1-e^2}} - \frac{(1-e)\cos iW_e}{n}\right)^2 + \frac{\cos^2\omega\sin^2 iW_e^2(1-e)^2}{n^2}\right]^{-1/2}. \tag{18}$$

C. Along-track/Cross-track Formations

A formation whose motion is entirely in the along-track/cross-track plane is achieved by requiring the radial position always be zero. Thus $\Delta e = \Delta M = 0$ and we are left with three design parameters to specify: $\Delta\omega$, Δi, and $\Delta\Omega$.

All along-track/cross-track formations resemble one of two types of motion in the along-track/cross-track plane. If the phase of the cross-track motion, φ_0, equals 90-deg, then Eqs. (10) – (12) describe a straight line with slope, s, equal to

$$|s| = \frac{\alpha}{e(\cos i\Delta\Omega + \Delta\omega)}.$$

The sign of s is determined by the position of the vehicle at perigee; if the vehicle is in the bottom half of the plane, s is positive and if the vehicle is in the top half of the plane, s is negative.

If φ_0 does not equal 90-deg, then Eqs. (10) – (12) describe an ellipse in the along-track/cross-track plane centered at $[a(\cos i\Delta\Omega + \Delta\omega), -ae\alpha]$.

To simplify our analysis, we restrict the vehicles to linear motion, and, thus, from Eq. (12) we have the constraint

$$\beta_{ACF} = \cos\omega\Delta i_{ACF} + \sin i \sin\omega\Delta\Omega_{ACF} = 0. \tag{19}$$

The remaining two design parameters characterize the size and shape of the formation at a particular time in the orbit. If we define the along-track and cross-track position at perigee to be y_0 and z_0, then we can immediately identify the other two conditions. From Eq. (10) we have,

$$\cos i\Delta\Omega_{ACF} + \Delta\omega_{ACF} = \frac{y_0}{a(1-e)}, \tag{20}$$

and, similarly, from Eq. (11) we have

$$\sin\omega\Delta i_{ACF} - \sin i\cos\omega\Delta\Omega_{ACF} = \frac{z_0}{a(1-e)}. \tag{21}$$

Special care must be taken when solving Eqs. (19) – (21) in equatorial (i = 0 or 180-deg) and polar (i = 90-deg) reference orbits, as well as when perigee of the reference orbit is located at a nodal crossing (ω = 0 or 180-deg). We solve one such case here. If the reference orbit is inclined ($i \neq 0$ or 180-deg) and perigee is located at a nodal crossing (ω = 0 or 180-deg), then Eqs. (19) – (21) are solved by

$$\Delta\Omega_{ACF} = -\frac{z_0}{a(1-e)\sin i}, \tag{22}$$

$$\Delta\omega_{ACF} = \frac{y_0 \sin i + z_0 \cos i}{a(1-e)\sin i}, \tag{23}$$

$$\Delta i_{ACF} = 0. \tag{24}$$

The minimum separation between any two vehicles in an along-track/cross-track formation is a function of the phasing angle between the vehicles. The phase, γ_f, of one vehicle with respect to another is

$$\gamma_f = \tan^{-1}\left(\frac{z_0}{y_0}\right).$$

If z_0/y_0 is less than or equal to $e^{1/2}$, then the minimum separation between the vehicles, $\rho_{\min}^{ACF}$, occurs at perigee ($\nu_{\min}^{ACF}$ = 0-deg) and is equal to

$$\rho_{\min}^{ACF} = \sqrt{y_0^2 + z_0^2}. \tag{25}$$

Otherwise, $\rho_{\min}^{ACF}$ occurs at

$$\nu_{\min}^{ACF} = \cos^{-1}\left(\frac{ey_0^2}{z_0^2}\right), \tag{26}$$

and is equal to

$$\rho_{\min}^{ACF} = \left|\frac{y_0 z_0 (e+1)}{\sqrt{e^2 y_0^2 + z_0^2}}\right|. \tag{27}$$

The maximum separation between any two vehicles, $\rho_{\max}^{ACF}$, always occurs at apogee ($\nu_{\max}^{ACF}$ = 180-deg) and is equal to

$$\rho_{\max}^{ACF} = \frac{1+e}{1-e}\sqrt{y_0^2 + z_0^2}. \tag{28}$$

Inspection of Eq. (27) reveals one important condition for along-track/cross-track formations: if $y_0 = 0$ then $\rho_{\min}^{ACF} = 0$ and a collision will occur at $\nu_{\min}^{ACF}$. Therefore, vehicles in along-track/cross-track formations cannot be aligned in the along-track direction at perigee.

V. Test Formations

This section examines the accuracy of the formation design methods discussed in the preceding sections. An example of each formation type is considered: (1) an along-track formation, (2) a follower formation, and (3) an along-track/cross-track formation. The motion of a deputy about a chief is examined for each test formation. The size of each test formation at perigee (i.e., the separation between the chief and deputy) is 1-km. Because the size of the relative motion is proportional to the size of the formation at perigee, the relative motion for a different sized formation is obtained by simply scaling the results in this section by the desired size of the formation at perigee.

Some of the characteristics of the relative motion are lost when the nonlinear equations of motion are linearized in the derivation of Eqs. (10) – (12). To evaluate the accuracy of Eqs. (10) – (12), a set of Keplerian elements is computed for each deputy using the design methods presented in this paper. The Keplerian elements of each deputy are converted to Earth-Centered-Inertial (ECI) coordinates, which are then propagated separately using simple two-body dynamics. These ECI coordinates serve as the 'true' position and velocity of the deputy. The true RAC position and velocity of the deputy are computed from the ECI coordinates using the following conversion,

$$\begin{aligned}
x_{true} &= r_{deputy} - r, \\
y_{true} &= r\theta_{true}^{y}, \\
z_{true} &= r\theta_{true}^{z}, \\
\dot{x}_{true} &= \dot{r}_{deputy} - \dot{r}, \\
\dot{y}_{true} &= \dot{r}\theta_{true}^{y} + r\dot{\theta}_{true}^{y}, \\
\dot{z}_{true} &= \dot{r}\theta_{true}^{y} + r\dot{\theta}_{true}^{y},
\end{aligned}$$

where x_{true}, y_{true}, and z_{true} are the true radial, along-track, and cross-track position of the deputy and $\dot{x}_{true}$, $\dot{y}_{true}$, and $\dot{z}_{true}$ are the true radial, along-track, and cross-track velocity of the deputy. The details of the ECI to RAC conversion are summarized in Appendix A.

The *position linearization error*, ε_p, is defined as the norm of the difference between the true RAC position and Eqs. (10) – (12),

$$\varepsilon_p = \sqrt{(x_{true} - x)^2 + (y_{true} - y)^2 + (z_{true} - z)^2}. \tag{29}$$

Similarly, the *velocity linearization error*, ε_v, is defined as the norm of the difference between the true RAC velocity and the derivatives of Eqs. (10) – (12), which are found in Appendix B,

$$\varepsilon_v = \sqrt{(\dot{x}_{true} - \dot{x})^2 + (\dot{y}_{true} - \dot{y})^2 + (\dot{z}_{true} - \dot{z})^2}. \tag{30}$$

Equations (29) and (30) are a measure of the information lost in Eqs. (10) – (12). It might be tempting to assume that Eqs. (29) and (30) occur independently of one another, but they are coupled. Both are a function of how nearby the deputy is to the chief in position *and* velocity; the key simplifying assumption in the derivation of Eqs. (10) – (12). This assumption is the main source of the linearization error and allows us to make an important observation: if you increase the size of the formation by an order of magnitude, you increase the linearization error by two orders of magnitude. Thus, the linearization error is proportional to the size of the formation squared.

The orbit of the chief in all three test formations is the reference orbit. Table 1 lists the Keplerian elements of the chief. The chief appears stationary in each formation because it is always at the origin of the RAC frame.

Table 1. Keplerian elements of chief in test formations.

Parameter	Chief
Perigee radius (r_p)	16,072-km
Apogee radius (r_a)	68,120-km
Semimajor axis (a)	42,096-km
Eccentricity (e)	0.6182
Inclination (i)	10-deg
Right ascension of ascending node (Ω)	0-deg
Argument of perigee (ω)	0-deg
Mean anomaly at epoch (M_0)	0-deg

A. Along-track Test Formation

The deputy only has an along-track component of motion in this formation. Using Eq. (13) and the values listed in Table 1, $\Delta\omega_{AF}$ is 0.00357-deg. All the other Keplerian element differences are zero.

The evolution of the formation in the radial/along-track plane is shown in Figure 3. The oscillatory motion of the deputy is illustrated in this figure. Figure 4 shows the true along-track position and velocity of the deputy. The true radial and cross-track position and velocity are zero within machine precision. In Fig. 4, the minimum separation between the vehicles is 1-km and the maximum separation is approximately 4.24-km. Equations (14) and (15) predict the true minimum and maximum separation within machine precision.

The position and velocity linearization errors for the deputy are always zero within machine precision. This is the result of the simple, linear motion of the deputy and the use of the curvilinear coordinate frame.

B. Follower Test Formation

Both vehicles share the same groundtrack in this formation, with the deputy following the chief. Using Eqs. (17) and (18) and the values listed in Table 1, ΔM_{FF} is −0.00081-deg and $\Delta\Omega_{FF}$ is 0.00081-deg. The other Keplerian element differences are zero.

The groundtrack of both vehicles is compared in Figure 5. The difference between the latitude and longitude of the chief at time t and the latitude and longitude of the deputy at time $t + \Delta M/n$ is zero within machine precision and, thus, the chief and deputy share identical groundtracks.

Figure 6 shows the true radial, along-track, and cross-track position and velocity of the deputy. Most of the motion of the deputy is contained in the radial/along-track plane, with only a slight cross-track motion. This is due to the small inclination of the orbit of the chief. As the inclination of the orbit of the chief increases, so does the magnitude of the cross-track motion.

Figure 7 shows the position and velocity linearization errors for the deputy for 5 orbital periods. In Fig. 7, both the position and velocity linearization errors are periodic and bounded. The maximum position linearization error is approximately 0.022-m, which is less than 0.006-percent of the minimum separation between the vehicles. The maximum velocity linearization error is approximately 0.014-mm/s. In Figure 8, the size of the formation at perigee is varied from 1-km to 100-km. The position linearization error is not significant for most applications, never exceeding 1-percent of the minimum vehicle separation for formation sizes less than 100-km.

C. Along-track/Cross-track Test Formation

The motion of the deputy in this formation is linear and contained in the along-track/cross-track plane. Figure 9 plots $\Delta\Omega_{ACF}$ and $\Delta\omega_{ACF}$, which were computed using Eqs. (22) and (23) and the values listed in Table 1, as a function of the phase of the deputy. The other Keplerian elements differences are zero.

The motion and evolution of the deputy in the along-track/cross-track plane for several different phases is shown in Figures 10 and 11. The straight-line motion of the deputy is illustrated in both figures. Figure 12 shows the true along-track and cross-track position and velocity of the deputy as a function of the phase of the deputy. The radial position and velocity is zero within machine precision. As we can see in Figs. 10 – 12, purely along-track motion results when the phase of the deputy is 0 or 180-deg (i.e., when $z_0 = 0$) and purely cross-track motion results when the phase of the deputy is 90 or 270-deg (i.e., when $y_0 = 0$). Purely along-track motion is discussed in section A and the vehicles collide when $y_0 = 0$, so the reminder of this section does not discuss the 0, 90, 180, or 270-deg cases. They are included on figures whenever necessary as envelopes of the relative motion.

Figure 13 shows the true separation between the vehicles as a function of the phase of the deputy. The maximum separation is independent of the phase and is approximately 4.24-km. The error in Eq. (28) is small, typically less than 10^{-4}-percent of the true value. If the phase of the deputy is less than or equal to $\tan^{-1}(e^{1/2})$, then the true minimum separation is approximately 1-km. The minimum separation predicted by Eq. (25) is also generally within 10^{-4}-percent of the true value. If the phase of the deputy is greater than $\tan^{-1}(e^{1/2})$, then the true anomaly at which the minimum separation occurs predicted by Eq. (26) and the minimum separation predicted by Eq. (27) are both typically within 0.01-percent of the true value.

The position and velocity linearization errors for the deputy as a function of the phase of the deputy for 5 orbital periods are shown in Figure 14. The interesting result is deputies with supplementary phases, such as 60 and 120-deg, have different linearization errors. At first, this seems inconsistent: the magnitude of the position and velocity for deputies with supplementary phases appears to be the same in Fig. 12 and, therefore, both deputies should have the same linearization error.

However, consider for a moment two deputies, one with a phasing of 60-deg (labeled *D1*) and one with as phasing of 120-deg (labeled *D2*). Figure 15 shows the cross-track components of the position and velocity linearization errors for *D1* and *D2*. Examination of Figs. 14 and 15 reveals that the cross-track components account for almost all the position and velocity linearization errors. This is due to a lack of symmetry in the cross-track motion of *D1* and *D2* that is not captured by Eqs. (10) – (12). According to Eqs. (10) – (12), the magnitude of the cross-track position and velocity of *D1* and *D2* are equal at every instant in time. This, however, is not realistic because *D1* is *ahead* of *D2* in its orbit. This causes *D1* and *D2* to have slightly different cross-track positions and velocities at every instant in time. Thus, the position and velocity linearization errors for *D1* and *D2*, and all deputies with supplementary phases, are different. This effect is also present in the along-track direction, but is more noticeable in the cross-track direction because of a greater lack of symmetry between the two orbits in this dimension. The along-track components of the linearization error are generally an order of magnitude smaller then the cross-track components.

The position and velocity linearization error for both deputies is again periodic and bounded in Fig. 14. The maximum position linearization error is always less than 0.4-m, which is approximately 0.15-percent of the minimum separation between the vehicles. The maximum velocity linearization error is always less than 0.08-mm/s. The size of the formation at perigee is varied from 1-km to 100-km in Figure 16. The position linearization error exceeds 1-percent of the minimum separation at a formation size of approximately 7-km.

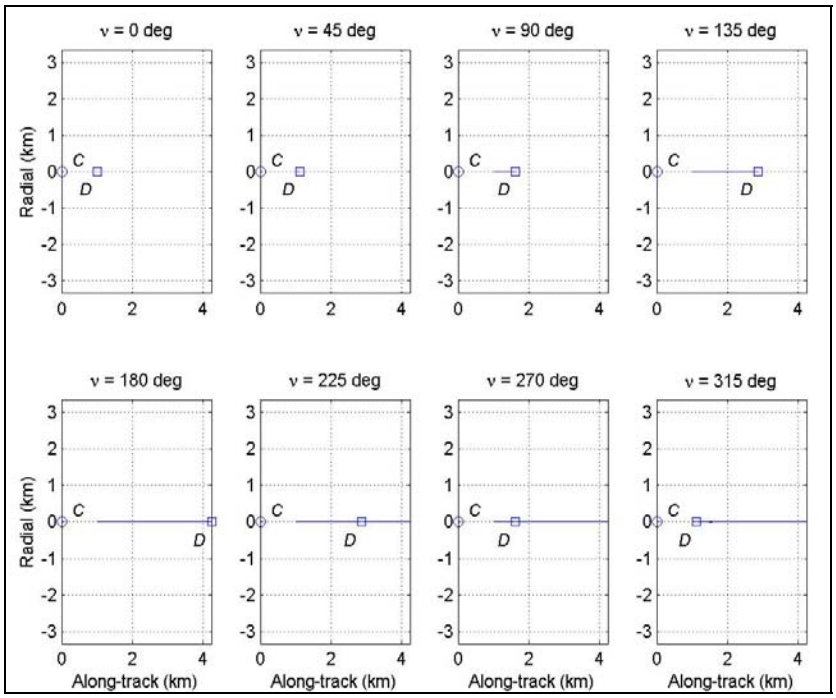

Figure 3. Evolution of deputy in along-track formation in radial/along-track plane.

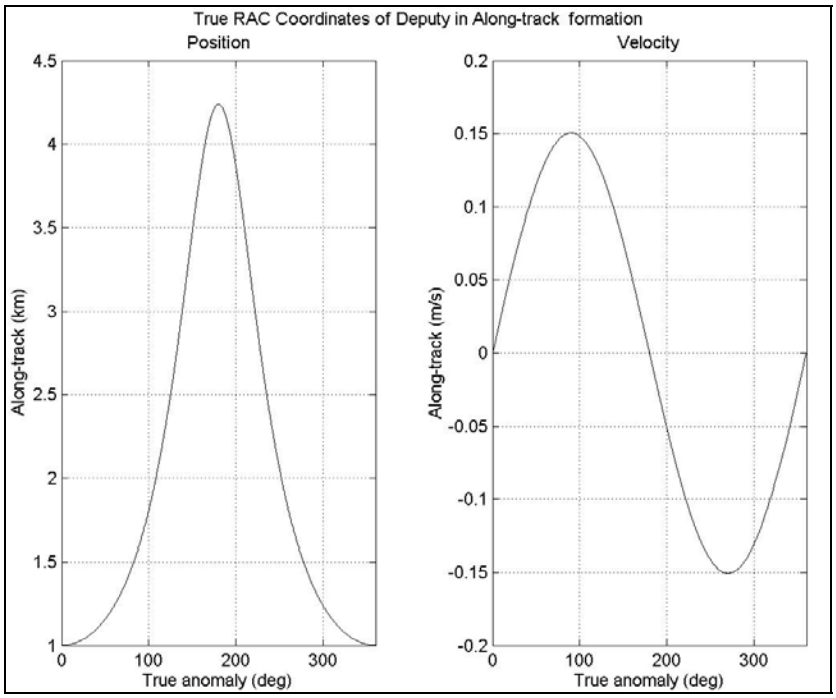

Figure 4. True RAC coordinates for along-track formation.

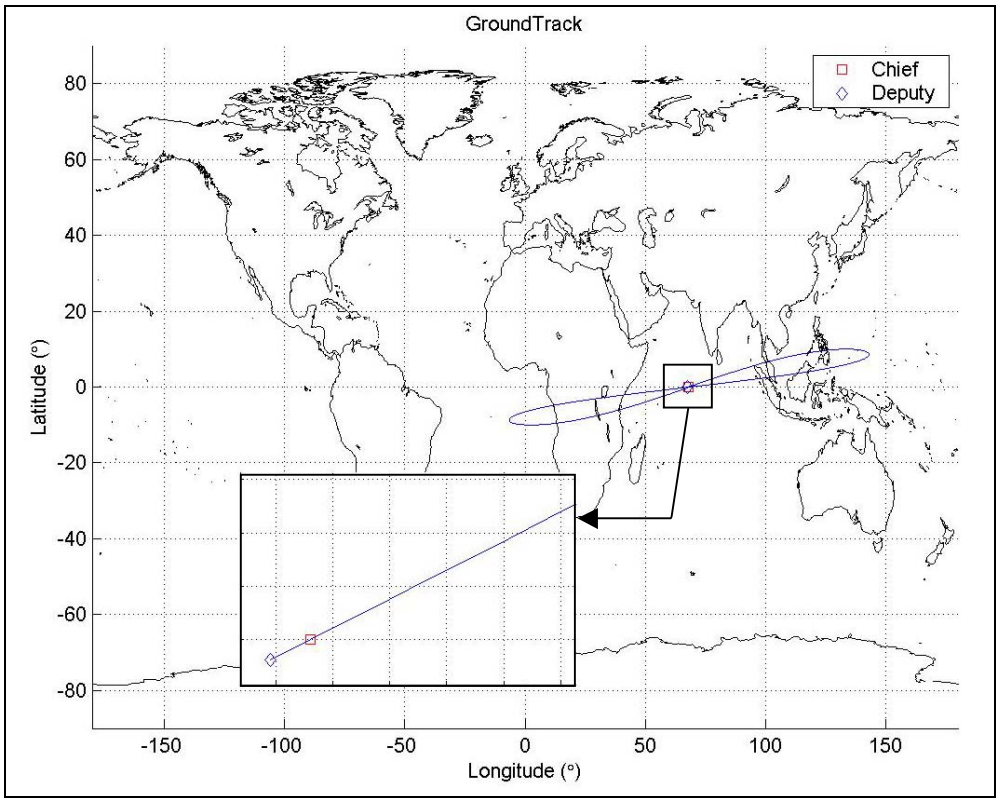

Figure 5. Groundtrack for follower formation.

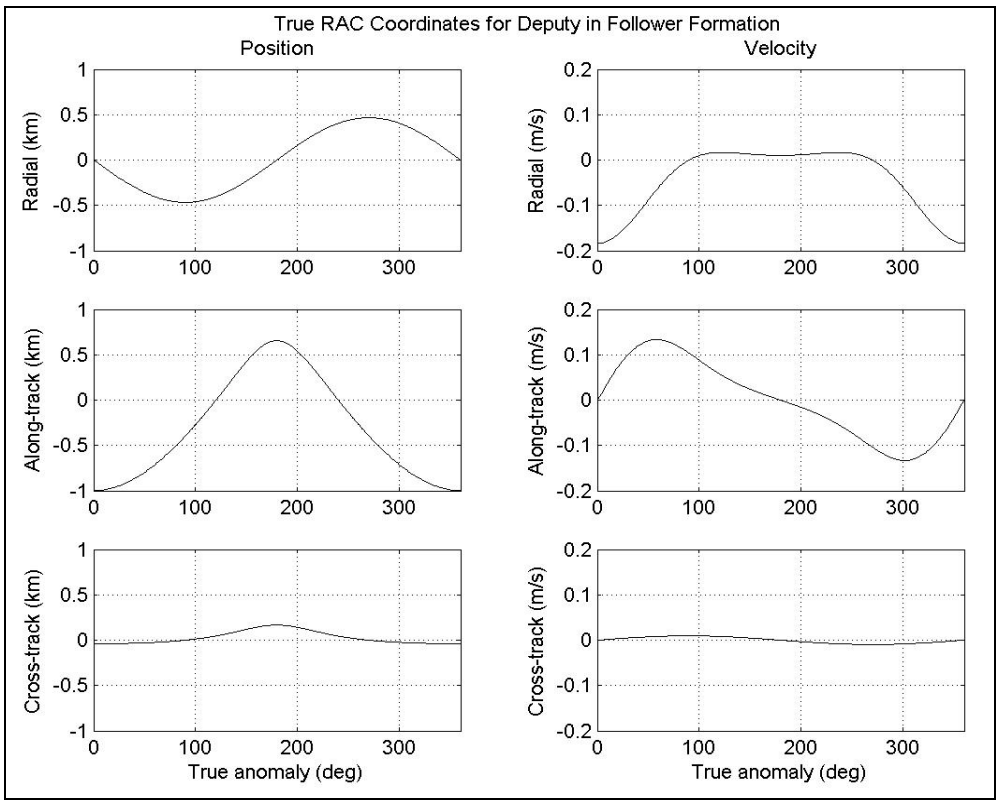

Figure 6. True RAC coordinates for follower formation.

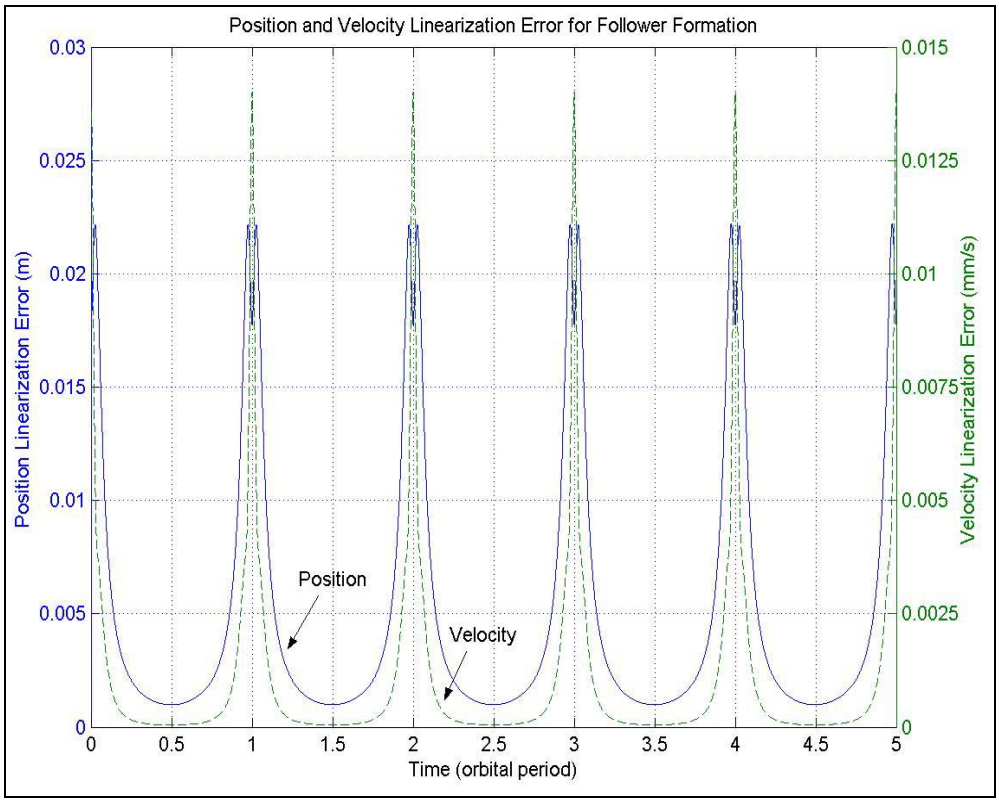

Figure 7. Linearization error for follower formation.

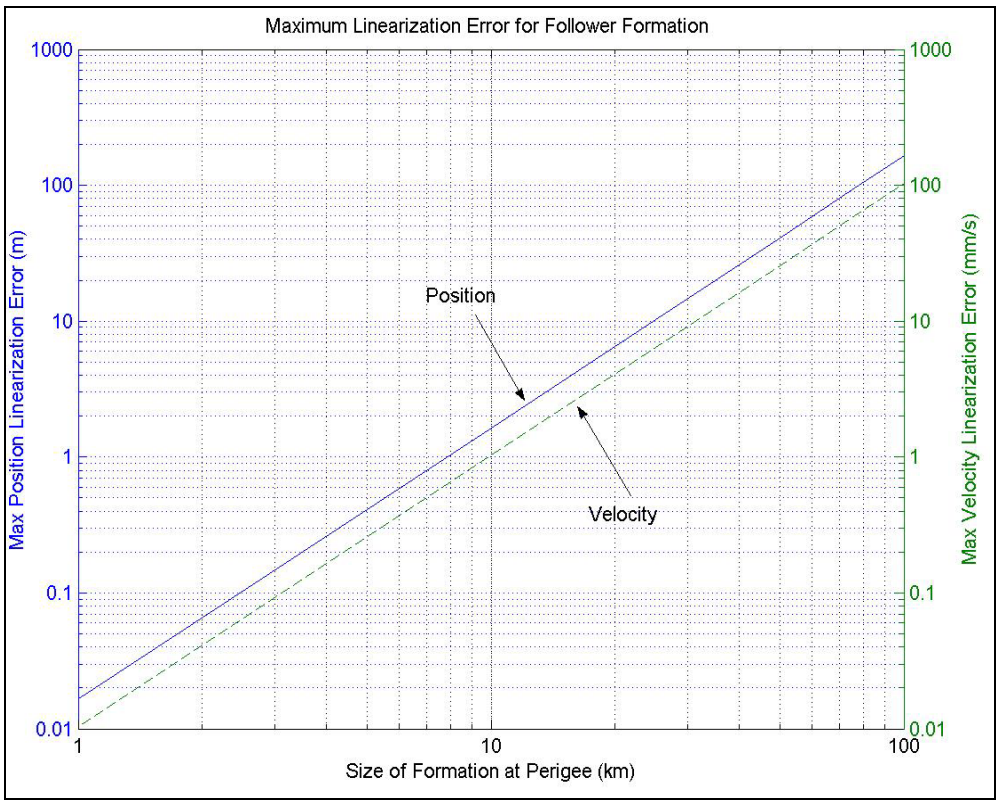

Figure 8. Maximum linearization error for follower formation.

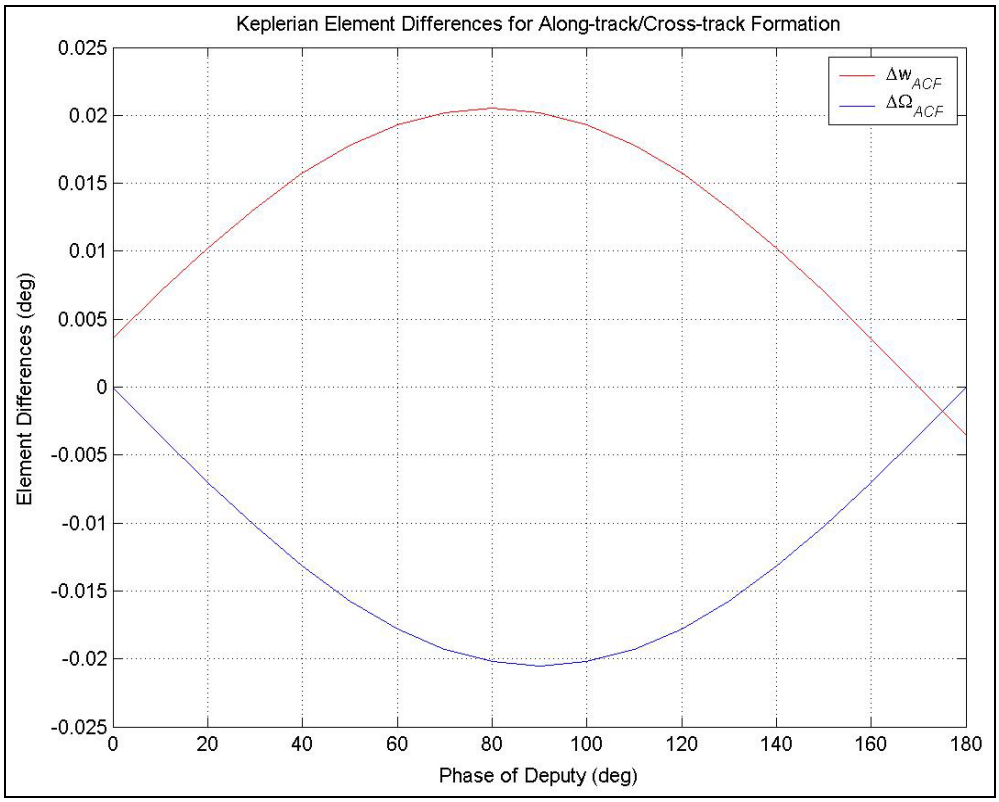

Figure 9. Keplerian element differences for along-track/cross-track formation.

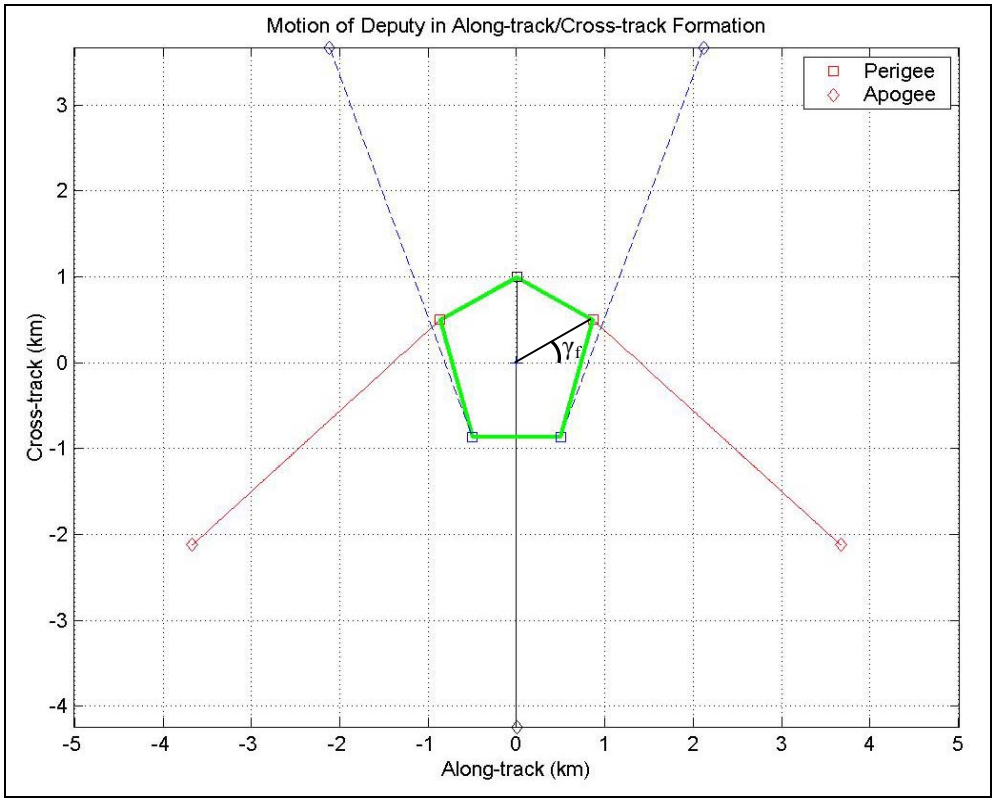

Figure 10. Motion of deputy in along-track/cross-track formation in along-track/cross-track plane.

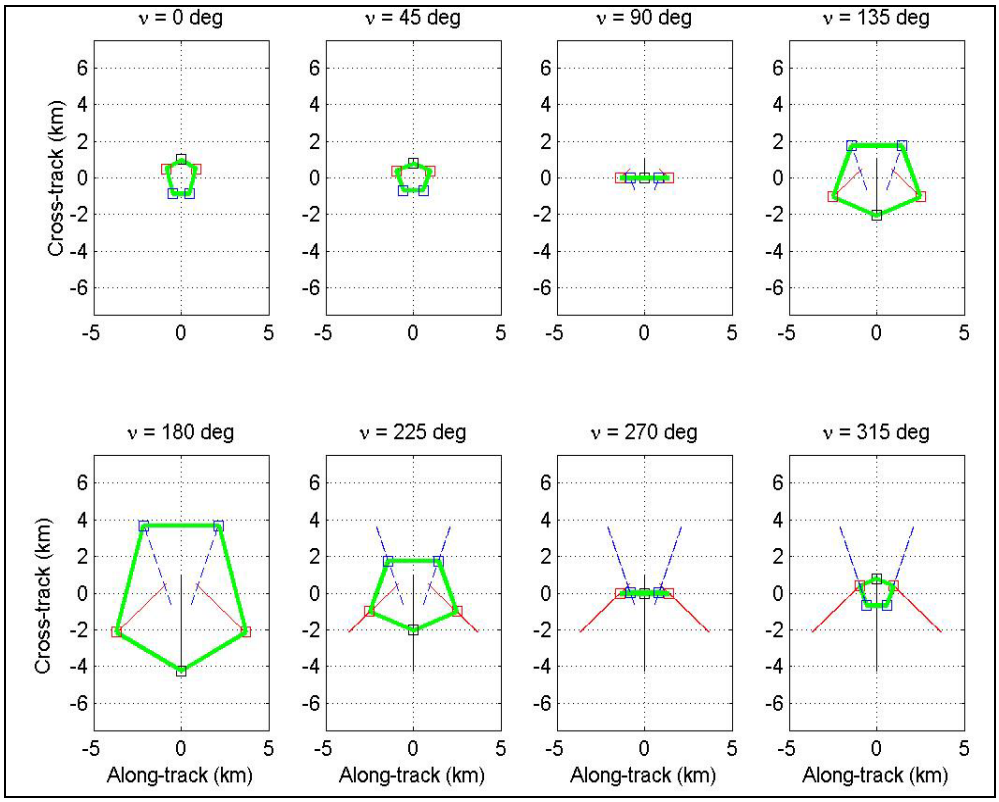

Figure 11. Evolution of deputy in along-track/cross-track formation in along-track/cross-track plane.

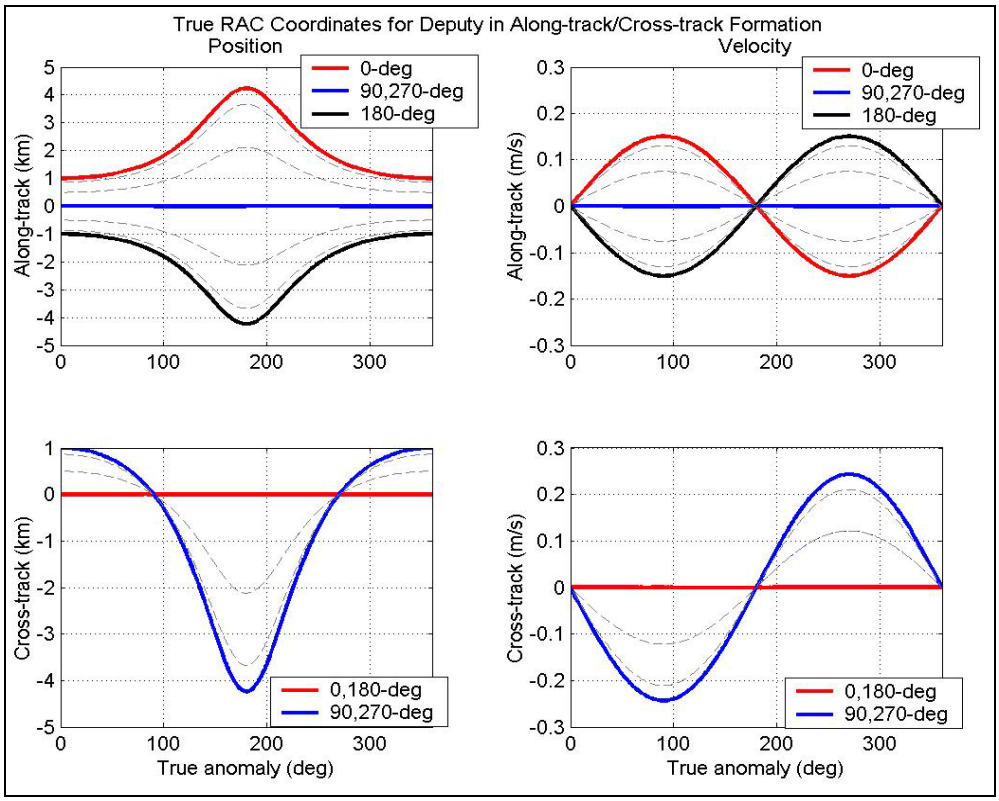

Figure 12. True RAC coordinates for along-track/cross-track formation.

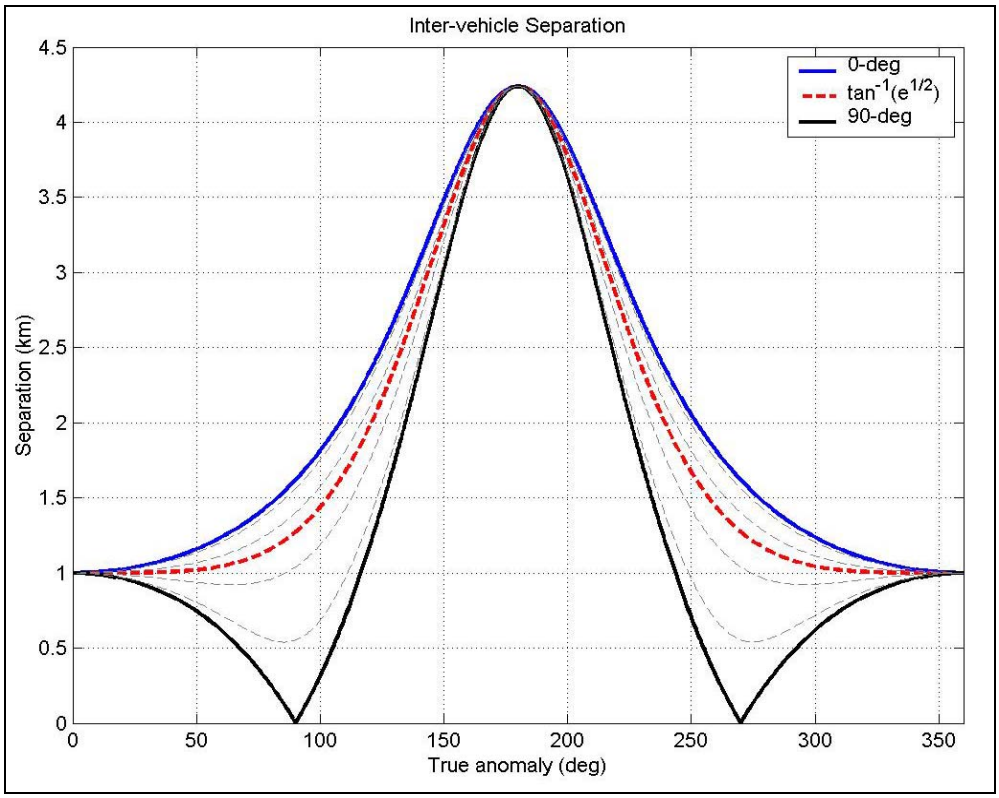

Figure 13. Inter-vehicle separation for along-track/cross-track formation.

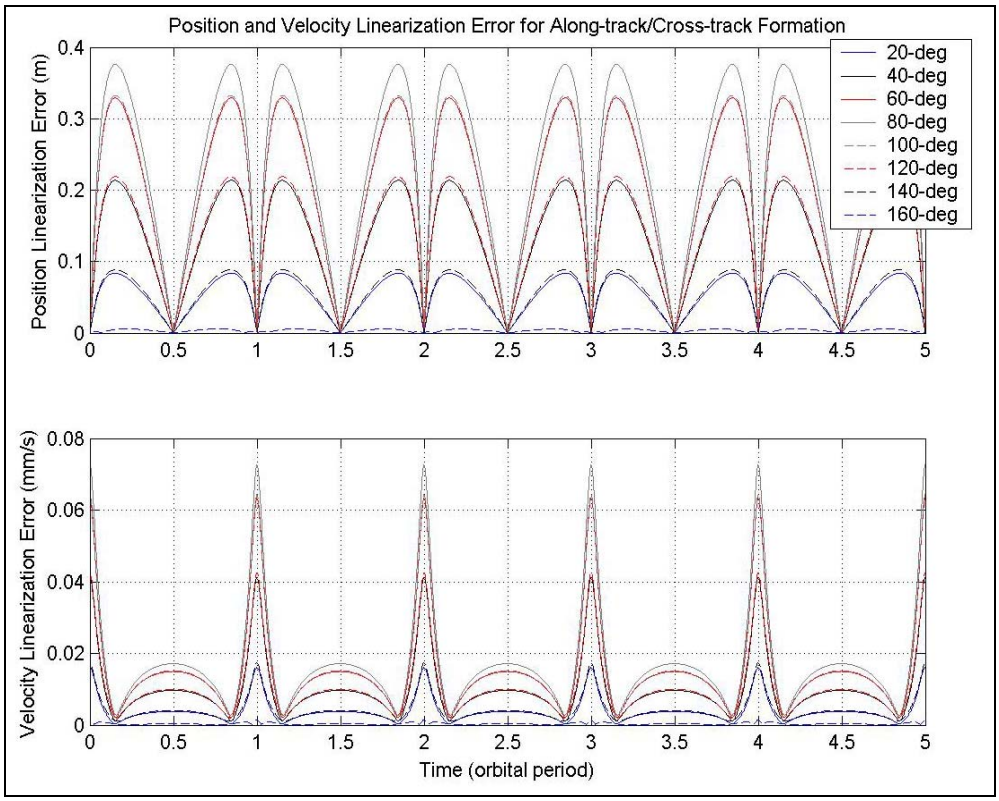

Figure 14. Linearization error for along-track/cross-track formation.

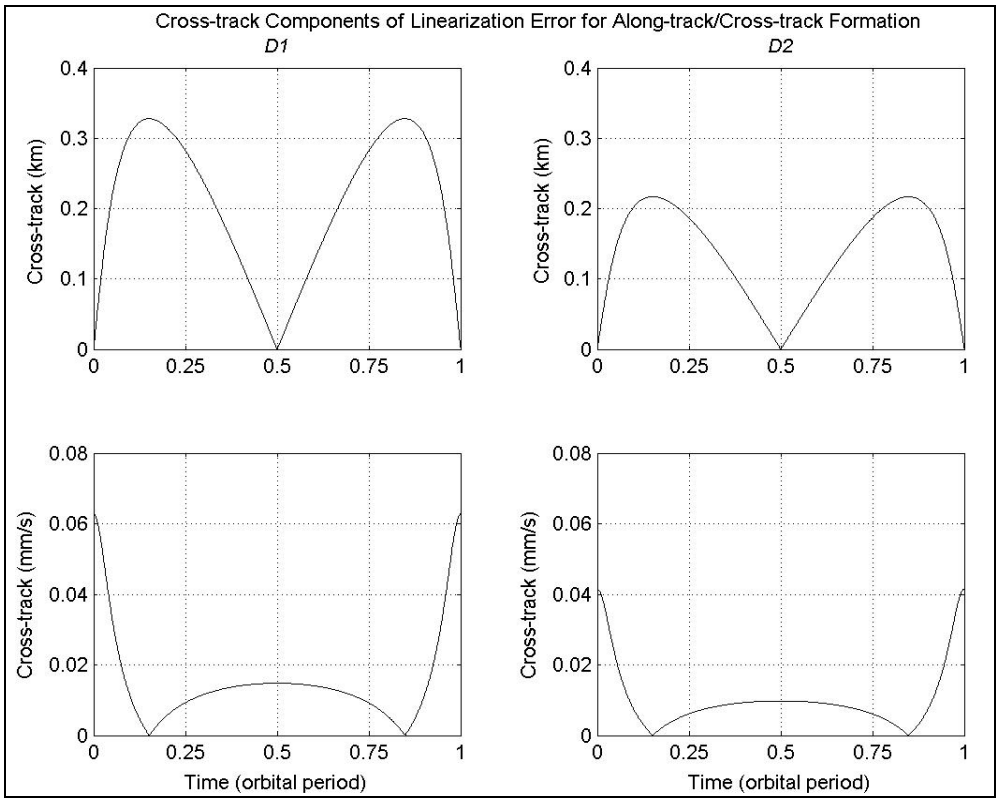

Figure 15. Cross-track components of linearization error for along-track/cross-track formation.

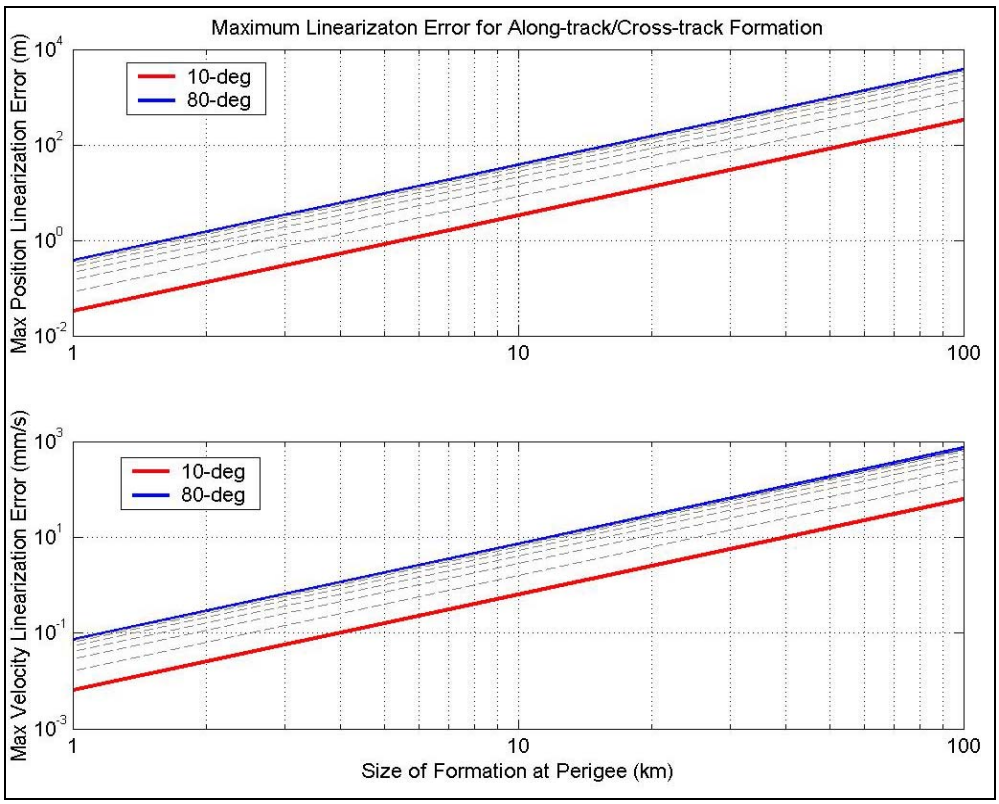

Figure 16. Maximum linearization error for along-track/cross-track formation.

VI. Conclusions

This paper developed and evaluated a set of geometrical relationships for formation flying design in eccentric orbits. Geometrical design methods are valuable for two reasons: (1) they provide a rapid method to design formation geometries and constraints to meet specific mission requirements and (2) they offer valuable insight into the characteristics of the relative motion. The geometrical relationships presented in this paper are based on the analytical solution to the linearized equations of relative motion in an eccentric reference orbit discussed in Ref. 2. Previous geometrical methods for formation design have been limited to near circular reference orbits, but we have avoided this restriction.

Three types of formations were analyzed: (1) an along-track formation, (2) a follower formation, and (3) an along-track/cross-track formation. Our formation design method proved to be a useful tool not only in the design of appropriate formation constraints, but also in understanding the characteristics and properties of the relative motion. The position linearization error was less than 0.4-m and the velocity linearization error was less than 0.08-mm/s for a 1-km formation at perigee.

The next steps will be to (1) evaluate the influence of perturbations and higher-order gravity terms on the motion, (2) use the results presented in this paper as a starting point for numerical optimization methods, and (3) employ Eqs. (10) – (12) in a relative navigation filter.

APPENDIX A: Rotating from ECI to RAC

If the ECI coordinates of the chief and deputy are known such that

$$\vec{r} = \begin{bmatrix} x_{ECI} & y_{ECI} & z_{ECI} \end{bmatrix},\ \dot{\vec{r}} = \begin{bmatrix} \dot{x}_{ECI} & \dot{y}_{ECI} & \dot{z}_{ECI} \end{bmatrix},$$
$$\vec{r}_{deputy} = \begin{bmatrix} x_{ECI} & y_{ECI} & z_{ECI} \end{bmatrix}_{deputy},\ \dot{\vec{r}}_{deputy} = \begin{bmatrix} \dot{x}_{ECI} & \dot{y}_{ECI} & \dot{z}_{ECI} \end{bmatrix}_{deputy},$$

then the RAC position and velocity of the deputy with respect to the chief is compute using the following conversion,

$$\vec{R} = \frac{\vec{r}}{|\vec{r}|},\ \dot{\vec{R}} = \frac{\dot{\vec{r}}}{|\vec{r}|} - \frac{\vec{r} \cdot \dot{\vec{r}}}{|\vec{r}|^3}\vec{r}$$

$$\vec{C} = \frac{\vec{r} \times \dot{\vec{r}}}{|\vec{r} \times \dot{\vec{r}}|},\ \dot{\vec{C}} = 0$$

$$\vec{A} = \vec{C} \times \vec{R},\ \dot{\vec{A}} = \vec{C} \times \dot{\vec{R}},$$

$$\vec{R}_{deputy} = \frac{\vec{r}_{deputy}}{|\vec{r}_{deputy}|},\ \dot{\vec{R}}_{deputy} = \frac{\dot{\vec{r}}_{deputy}}{|\vec{r}_{deputy}|} - \frac{\vec{r}_{deputy} \cdot \dot{\vec{r}}_{deputy}}{|\vec{r}_{deputy}|^3}\vec{r}_{deputy},$$

$$\theta_y = \sin^{-1}\left(\vec{R}_{deputy} \cdot \vec{A}\right),\ \dot{\theta}_y = \frac{\vec{R}_{deputy} \cdot \dot{\vec{A}} + \dot{\vec{R}}_{deputy} \cdot \vec{A}}{\cos\theta_y},$$

$$\theta_z = \sin^{-1}\left(\vec{R}_{deputy} \cdot \vec{C}\right),\ \dot{\theta}_z = \frac{\dot{\vec{R}}_{deputy} \cdot \vec{C}}{\cos\theta_z},$$

$$x = |\vec{r}_{deputy}| - |\vec{r}|,\ \dot{x} = \frac{\vec{r}_{deputy} \cdot \dot{\vec{r}}_{deputy}}{|\vec{r}_{deputy}|} - \frac{\vec{r} \cdot \dot{\vec{r}}}{|\vec{r}|},$$

$$y = |\vec{r}|\theta_y,\ \dot{y} = \frac{\vec{r} \cdot \dot{\vec{r}}}{|\vec{r}|}\theta_y + |\vec{r}|\dot{\theta}_y,$$

$$z = |\vec{r}|\theta_z,\ \dot{z} = \frac{\vec{r} \cdot \dot{\vec{r}}}{|\vec{r}|}\theta_z + |\vec{r}|\dot{\theta}_z,$$

where x, y, and z are the radial, along-track and cross-track position of the deputy with respect to the chief, and $\dot{x}$, $\dot{y}$, and $\dot{z}$ are the radial, along-track and cross-track velocity of the deputy with respect to the chief.

APPENDIX B: The velocity equations

The velocity equations are obtained by taken the time derivative of Eqs. (7) – (9),

$$\dot{x} = n \sin\nu \sqrt{1-e^2} \left(\frac{a^3}{r^2} \right) \Delta e + en \cos\nu \left(\frac{a^3}{r^2} \right) \Delta M,$$

$$\dot{y} = \left(n\sqrt{1-e^2} \left(1 + \frac{r}{p} \right) \left(\frac{a^3}{r^2} \right) \cos\nu + \frac{en \sin^2 \nu}{\left(1-e^2\right)^{3/2}} \right) \Delta e - en \sin\nu \left(\frac{a^3}{r^2} \right) \Delta M + \frac{aen \sin\nu}{\sqrt{1-e^2}} \Delta\omega + \frac{aen \cos i \sin\nu}{\sqrt{1-e^2}} \Delta\Omega,$$

$$\dot{z} = \frac{an}{\sqrt{1-e^2}} \left(\sin i \left(\sin\theta + e \sin\omega \right) \Delta\Omega + \left(\cos\theta + e \cos\omega \right) \Delta i \right).$$

Acknowledgments

This work was funded under Cooperative Agreement NCC5-721 through the NASA GSFC Formation Flying NASA Research Announcement. Any opinions, findings, and conclusions or recommendations expressed in this material are those of the authors and do not necessarily reflect the views of the National Aeronautics and Space Administration.

The authors would like to thank Mike Moreau, Russell Carpenter, and Steven Hughes of NASA Goddard Space Flight Center for their insights and suggestions.

References

[1]Alfriend, K.T. and H. Yan, "An Evaluation and Comparison of Relative Motion Theories," AAS/AIAA Astrodynamics Specialist Conference, August 3-7, 2003, Big Sky, MT, Paper AAS 03-567.

[2]Broucke, Roger A., "Solution of the Elliptic Rendezvous Problem with the Time as Independent Variable," *Journal of Guidance, Control, and Navigation*, Vol. 26, No. 4, 2003, pp. 615 – 621.

[3]Gim, D.W. and K.T. Alfriend, "The State Transition Matrix of Relative Motion for the Perturbed Non-Circular Reference Orbit," Proceedings of the AAS/AIAA Space Flight Mechanics Meeting, Feb 11-15, 2001, Santa Barbara, CA, Spaceflight Mechanics 2001, *Advances in the Astronautical Sciences*, Vol. 108, Part I, pp 913-934, 2001.

[4]Hill, G.W., "Researches in the Lunar Theory," American Journal of Mathematics, Vol. 1, 1878, pp 5 – 26, 129 – 147, 245 – 260.

[5]Hughes, S.P, "Formation Tetrahedron Design for Phase I of the Magnetospheric Multiscale Mission," Proceedings of the 2004 Flight Mechanics Symposium, NASA Goddard Space Flight Center, October 2003.

[6]Lawden, D.F., "Optimal Trajectories for Space Navigation," Butterworth, London, 1963, Chap. 5.

[7]Lovell, T.A. and S.G. Tragesser, "Analysis of the Reconfiguration and Maintenance of Close Spacecraft Formations," AAS/AIAA Astrodynamics Specialist Conference, August 3-7, 2003, Big Sky, MT, Paper AAS 03-139.

[8]Melton, R.G., "Time-Explicit Representation of Relative Motion Between Elliptical Orbits," *Journal of Guidance, Control, and Dynamics*, Vol. 23, No. 4, July – August 2000.

[9]Sabol, C., R. Burns, and C.A. McLaughlin, "Satellite Formation Flying Design and Evolution," *Journal of Spacecraft and Rockets*, Vol. 38, No. 2, March – April 2001, pp. 270-278.

[10]Schweighart, S.A., and R.J. Sedwick, "High-Fidelity Linearized J_2 Model for Satellite Formation Flight," *Journal of Guidance, Control, and Dynamics*, Vol. 25, No. 6, November – December 2002, pp. 1073-1080.

[11]Tschauner, J. and P. Hempel, "Optimale Beschleunigungs-propgramme fur des rendezvous Manover," *Astronautica Acta*, Vol. 10, Nos. 5 – 6, 1964, pp. 296 – 307.

[12]Vallado, D.A., "Fundamentals of Astrodynamics and Applications," published as part of the Space Technology Series by the McGraw-Hill Companies, Inc., College Custom Series, 2001, pp. 381 – 384.